PASJ: Publ. Astron. Soc. Japan **64**, 118, 2012 October 25

Optimization by Smoothed Bandpass Calibration in Radio Spectroscopy

Haruka YAMAKI, Seiji KAMENO,* Hirohisa BEPPU, Izumi MIZUNO, and Hiroshi IMAI
Department of Physics and Astronomy, Graduate School of Science and Engineering, Kagoshima University, 1-21-35 Korimoto, Kagoshima, Kagoshima 890-0065
kameno@sci.kagoshima-u.ac.jp

(Received 2012 March 21; accepted 2012 May 17)

Abstract

We have developed the Smoothed Bandpass Calibration (SBC) method and the best suitable scan pattern to optimize radio spectroscopic observations. Adequate spectral smoothing is applied to the spectrum toward OFF-source blank sky adjacent to a target source for the purpose of bandpass correction. Because the smoothing process reduces noise, we can reduce the integration time for OFF-source scans while keeping the signal-to-noise ratio. Since smoothing is not applied to ON-source scans, the spectral resolution for line features is maintained. An optimal smoothing window is determined by the bandpass flatness evaluated by the spectral Allan variance (SAV). An efficient scan pattern is designed for OFF-source scans within the bandpass-stability time scale estimated by the time-based Allan variance (TAV). We tested the SBC using a digital spectrometer, VESPA, at the VERA Iriki station. For a targeted noise level of 5×10^{-4} as its ratio to the system noise, the optimal smoothing window was 32–60 channels (ch) over the whole bandwidth of 1024 ch, and the optimal scan pattern was designed as a sequence of 70 s ON + 10 s OFF scan pairs. The noise level by the SBC has been improved by a factor of 1.74, compared with that by the conventional method. The total telescope-time to reach our target with the SBC was 400 s, which is 1/3 of 1200 s required in the conventional way. Improvements in the telescope-time efficiency with the SBC were calculated to be 3× (for single-beam scans), 2× (dual-beam), and 1.3× (on-the-fly). The SBC is useful for optimizing scan patterns for observations from now on, and also for improving the signal-to-noise ratios of archival data if ON- and OFF-source spectra are separately recorded, though the efficiency depends on the spectral stability of the receiving system.

Key words: instrumentation: detectors — methods: statistical — techniques: miscellaneous — techniques: spectroscopic — telescopes

1. Introduction

Spectral observations in radio astronomy aim to detect emission- or absorption-line features that bring us rich information, such as intensity, velocity, line width, etc. To acquire a spectrum, signals received by a radio telescope are processed in a spectrometer. The performance of a spectral observation is characterized by the spectral resolution, bandwidth, sensitivity, and stability.

A certain bandpass calibration procedure is needed to obtain a desired performance of spectral observations. An acquired spectrum is a summation of undesirable noises, $T_{\rm sys}$, and a signal from the target source, which is denoted as the antenna temperature, $T_{\rm a}(\nu)$. The spectral shape is affected by the bandpass response, $H(\nu)$, that is a transfer function of the receiving system as a function of the frequency, ν. The acquired ON-source spectrum will then be

$$T_{\rm ON}(\nu) = H(\nu)[T_{\rm sys} + T_{\rm a}(\nu)]. \tag{1}$$

A bandpass calibration is necessary to estimation of $T_{\rm a}(\nu)$ from the acquired spectrum, $T_{\rm ON}(\nu)$.

In most radio observations, the acquired spectrum is dominated by the system noise, i.e., $T_{\rm sys} \gg T_{\rm a}(\nu)$. To relieve the system noise, a spectrum of OFF-source blank sky adjacent to the target source is subtracted from the ON-source spectrum. This position-switching scan yields the source spectrum as

$$T_{\rm a}(\nu) = \frac{T_{\rm ON}(\nu) - T_{\rm OFF}(\nu)}{H(\nu)}, \tag{2}$$

where $T_{\rm OFF}(\nu)$ is the spectrum taken from the OFF-source scan. In conventional position-switching observations, the bandpass $H(\nu)$ is also acquired from OFF-source scans because the blank sky emits a featureless flat spectrum. For $H(\nu) = T_{\rm OFF}(\nu)/T_{\rm sys}$, equation (2) will be

$$T_{\rm a}(\nu) = T_{\rm sys}\left[\frac{T_{\rm ON}(\nu)}{T_{\rm OFF}(\nu)} - 1\right]. \tag{3}$$

The sensitivity of spectal observations is evaluated by the standard deviation, σ, of the acquired spectrum in line-free channels. It is derived from equation (3); that is,

$$\left[\frac{\sigma}{T_{\rm a}(\nu) + T_{\rm sys}}\right]^2 = \left[\frac{\sigma_{\rm ON}}{T_{\rm ON}(\nu)}\right]^2 + \left[\frac{\sigma_{\rm OFF}}{T_{\rm OFF}(\nu)}\right]^2, \tag{4}$$

where $\sigma_{\rm ON}$ and $\sigma_{\rm OFF}$ are the standard deviations of the ON- and OFF-source spectra, respectively. For weak sources for which $T_{\rm ON}(\nu) \simeq T_{\rm OFF}(\nu)$, σ is given by a root of the sum squared of $\sigma_{\rm ON}$ and $\sigma_{\rm OFF}$. When $\sigma_{\rm ON}$ and $\sigma_{\rm OFF}$ are dominated by the thermal noise, according to Wilson, Rohlfs, and Hüttemeister (2009), they are related to the integration times,

* Corresponding author: Seiji KAMENO.

$t_{\rm ON}$ and $t_{\rm OFF}$, the spectral resolution, $\nu_{\rm res}$, and $T_{\rm sys}$ in the following:

$$\sigma_{\rm ON} = \frac{T_{\rm sys} + T_{\rm a}}{\sqrt{\nu_{\rm res} t_{\rm ON}}},\ \sigma_{\rm OFF} = \frac{T_{\rm sys}}{\sqrt{\nu_{\rm res} t_{\rm OFF}}}. \quad (5)$$

The total telescope time is a sum of $t_{\rm ON}$, $t_{\rm OFF}$, and other overhead time, such as setup, system noise measurement, gaps between scans, etc. The optimized scan pattern is designed to maximize the sensitivity, i.e., to minimize σ, within the minimal telescope time. Conventionally, $t_{\rm ON}$ and $t_{\rm OFF}$ are equally allocated in position-switching observations to have $\sigma_{\rm ON} \simeq \sigma_{\rm OFF}$. This manner makes the total telescope time longer than twice of $t_{\rm ON}$ and lets $\sigma \simeq \sqrt{2}\sigma_{\rm ON}$.

If there is an efficient way to reduce $\sigma_{\rm OFF}$ less than $\sigma_{\rm ON}$, we can save the total telescope time and obtain better sensitivity. For an ideal receiving system, whose bandpass responses were known *a priori* and to be very stable, OFF-source observations would be unnecessary. Modern systems offer better spectral stability in the trend to replace analog devices with a high-speed digital sampling system in an upper stream of signal transfer. The bandpass response of a digital system, including a digital filter and a digital spectrometer, is determined by a fixed algorithm, and is not affected by environmental variations. The utility of digital devices hold the possibility of reducing the integration time and the standard deviation of OFF-source scans.

In this paper we propose the Smoothed Bandpass Calibration (SBC) method by which the OFF-source spectrum is smoothed across the bandwidth so as to reduce the integration time of the OFF-source scan and the standard deviation of the spectrum. Section 2 describes the concept of the SBC method. Section 3 reports on test experiments that have been carried out in order to verify the SBC and to quest for optimal parameters of a smoothing window and a scan pattern. In section 4 we discuss the behavior of spectral stability and estimate the sensitivity improvement expected in some scan patterns.

2. Method

We propose the relevant spectral smoothing along the frequency for OFF-source scans to reduce the required integration time, so that it enables us to achieve a desired standard deviation. Before spectral smoothing, a bandpass correction is made by using a template bandpass response that is presumed to be relevantly static and taken by long-time integration toward the blank sky. The bandpass-corrected OFF-source spectrum will be almost flat with a slight warp due to fluctuation of the receiving system and is smeared by thermal noise. In the following subsections we formulate the spectral behavior and develop a new method for the reduction of spectral unevenness.

2.1. Description and Assumption

As described in section 1, the purpose of OFF-source scans is to subtract $T_{\rm sys}$ and to calibrate the bandpass, $H(\nu)$, which is a frequency-dependent system response. Since the bandpass can be time-variable, we denote it by

$$H(\nu, t) = H_0(\nu) + H_1(\nu, t), \quad (6)$$

where $H_0(\nu)$ is a static template bandpass and $H_1(\nu, t)$ is a fluctuation from $H_0(\nu)$. The observed OFF-source spectrum is composed of not only $H(\nu, t)$, but also thermal noise, $\epsilon(\nu, t)$, which is assumed to be attributed to a stochastic random process following the normal distribution with the mean, $\mu = 0$, and the variance, $\sigma^2_{\rm noise} = 1/(\nu_{\rm res} t_{\rm integ})$, where $t_{\rm integ}$ is the integration time. Thus, the observed OFF-source spectrum will be

$$T_{\rm OFF}(\nu, t) = [H_0(\nu) + H_1(\nu, t)]T_{\rm sys}[1 + \epsilon(\nu, t)], \quad (7)$$

and its expectation will be

$$\langle T_{\rm OFF}(\nu, t)\rangle = [H_0(\nu) + H_1(\nu, t)]T_{\rm sys}. \quad (8)$$

A sufficiently long integration time is required for conventional OFF-source scans to reduce $\sigma_{\rm noise}$.

We assume that $H_1(\nu, t)$ is relatively smaller than $H_0(\nu)$, almost flat and smooth along the frequency, with a typical frequency scale of variation, $\nu_{\rm var}$. Relevant spectral smoothing for OFF-source spectra efficiently reduces $\sigma_{\rm noise}$ by a factor of $\sqrt{(\nu_{\rm res}/\nu_{\rm var})}$, and keeps the expectation of the OFF-source spectrum. Since spectral smoothing will not be applied to ON-source spectra, the desired spectral resolution will be maintained.

2.2. Allan Variance Decomposition

The flatness of $H_1(\nu, t)$ is evaluated by the spectral Allan variance (SAV) analysis. The SAV is defined as

$$\sigma^2_{\rm y}(\Delta\nu) = \left\langle \frac{[H(\nu + \Delta\nu) - 2H(\nu) + H(\nu - \Delta\nu)]^2}{2\Delta\nu^2} \right\rangle, \quad (9)$$

where the angle bracket means the expectation. In a small frequency span ($\Delta\nu \ll \nu_{\rm var}$) the SAV is dominated by the thermal noise, and follows the characteristics of $\sigma^2_{\rm y}(\Delta\nu) \propto \Delta\nu^{-2}$. In a larger frequency span ($\Delta\nu \gg \nu_{\rm var}$), $H_1(\nu, t)$ exceeds the thermal noise and the characteristics of the SAV are different from those of the thermal noise. The SAV analysis allows us to separate $H_1(\nu, t)$ from the thermal noise.

An example of SAV for an OFF-source spectrum is shown in figure 1, as a function of the channel spacing, $\nu_{\rm sp}$.[1] The SAV in the 1 min integrated raw spectrum (*a*) is decomposed into two components: (1) thermal noise, $\epsilon(\nu, t)$, which dominates in the range of $\Delta\nu/\nu_{\rm sp} < 5$ and whose SAV has a dependence, $\Delta\nu^{-2}$, and (2) bandpass characteristics, $H(\nu, t)$, which dominate in the range of $\Delta\nu/\nu_{\rm sp} > 5$. When these two components show approximately symmetric power-law characteristics, the bottom of the SAV appears at the frequency span where these two components are almost equivalent (see results in subsection 3.2 and discussions in subsection 4.1). After a bandpass correction using the template spectrum, $H_0(\nu)$, the second component is considerably eliminated as shown in (*b*). The rest fluctuation, $H_1(\nu, t)$, dominates the SAV in $\Delta\nu/\nu_{\rm sp} > 120$. As the thermal noise will be reduced via the time integration in (*c*), the bottom of the SAV shifts to smaller $\Delta\nu$ (e.g., $\Delta\nu/\nu_{\rm sp} \sim 40$ for 546 min integration). The relevant spectral smoothing with its window given by the bottom in SAV, as described in the next

[1] As described in section 3, we used an FX spectrometer the spectral resolution function of which is a squared sinc function and $\nu_{\rm sp} = \nu_{\rm res}$ by 2048-point Fast Fourier Transform (FFT) to produce 1024 ch.

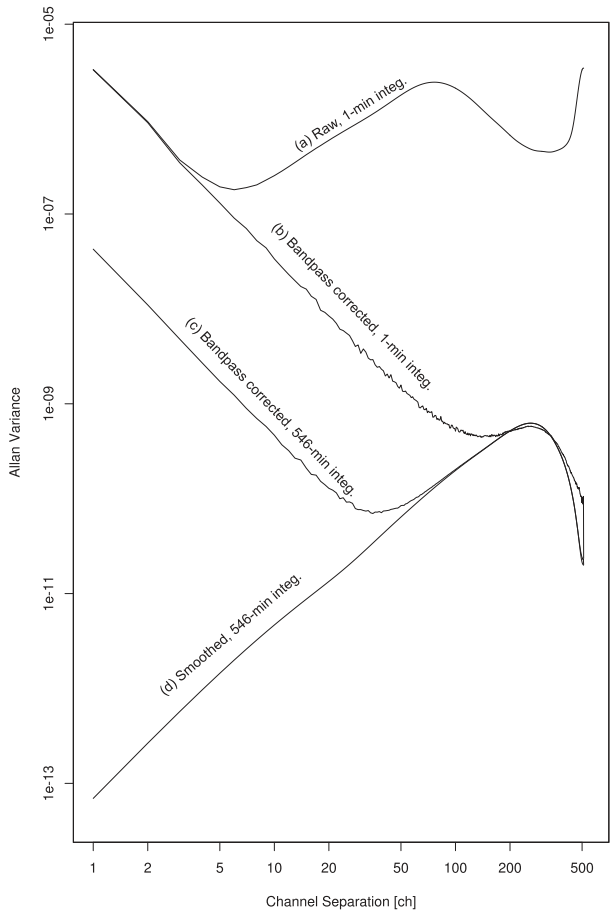

Fig. 1. Spectral Allan variance (SAV) across the 16 MHz bandwidth with 1024 spectral channels. The data comes from the field test described in section 3. Four SAV profiles are derived from (a) 1 min integrated raw spectrum before bandpass correction, (b) 1 min integrated spectrum after bandpass correction, (c) 546 min integrated spectrum after bandpass correction, and (d) 546 min integrated spectrum after bandpass correction and spline smoothing are applied.

subsection, will yield efficient reduction of the thermal noise, while keeping the bandpass response as shown in (*d*).

2.3. Strategy of Adequate Smoothing and Scans

The relevant smoothing window and ON-OFF scan pattern should be determined to minimize the standard deviation in the OFF-source-subtracted spectrum within a given telescope time, or to minimize the total telescope time that prevents the standard deviation from rising more than a given value. The best smoothing window, $N_{\rm sw} = \Delta\nu/\nu_{\rm res}$, is determined by the bottom of the SAV. After we apply the spectral smoothing to the OFF-source spectra, their variance is expected to be reduced to $\sigma^2_{\rm OFF}/N_{\rm sw}$.

Because of the inequality in variances of ON- and OFF-source spectra, we need to redesign the best duty cycles of $t_{\rm ON}$ and $t_{\rm OFF}$ under the condition where the total telescope time is constant. Let an ON-to-OFF-source integration time ratio be set to $(1-x)$:x in each of the duty cycle and the total telescope time of $t_{\rm tot}$.[2] Substituting $t_{\rm ON}$ with $(1-x)t_{\rm tot}$ and $t_{\rm OFF}$ with $xt_{\rm tot}$, and assuming that $T_{\rm a} \ll T_{\rm sys} \simeq T_{\rm ON} \simeq T_{\rm OFF}$ in equations (4) and (5), we have

$$\left(\frac{\sigma}{T_{\rm sys}}\right)^2 = \frac{1}{\nu_{\rm res} t_{\rm tot}}\left(\frac{1}{1-x} + \frac{1}{N_{\rm sw}x}\right). \quad (10)$$

The variance is minimized to

$$\left(\frac{\sigma_{\rm min}}{T_{\rm sys}}\right)^2 = \frac{1}{\nu_{\rm res} t_{\rm tot}}\frac{(1+\sqrt{N_{\rm sw}})^2}{N_{\rm sw}}, \quad (11)$$

when we have $x = 1/(1+\sqrt{N_{\rm sw}})$. When $N_{\rm sw} = 45$ for instance, the best ratio is 0.87:0.13.

The interval between adjacent OFF-source scans should be shorter than the time scale of the spectral stability in the receiving system. The spectral stability is evaluated by the time-based Allan variance (TAV). As can be seen in figure 3, a typical spectral shape of $H_1(\nu, t)$ shows an S-shaped feature with a peak and a bottom. Since we focus on the stability of the bandpass shape, the TAV is calculated by the difference between the levels of the peak and the bottom, i.e.,

$$\Delta H_1(t) = H_1(\nu_{\rm peak}, t) - H_1(\nu_{\rm bottom}, t). \quad (12)$$

Thus, the TAV is derived; that is,

$$\sigma^2_{\rm y}(\tau) = \left\langle \frac{[\Delta H_1(t+\tau) - 2\Delta H_1(t) + \Delta H_1(t-\tau)]^2}{2\tau^2} \right\rangle, \quad (13)$$

where τ is the time lag. The stability time scale is determined by the time lag, where the TAV follows $\sigma^2_{\rm y}(\tau) \propto \tau^{-2}$.

In summary, our strategy of determining the optimal spectral smoothing window and the scan pattern will be:

1. Acquire the template bandpass response, $H_0(\nu)$, and its dependence on a frequency band by sufficiently long integration before programed observations (e.g., during the seasonal maintenance). The relevant spectral smoothing can be applied to the template bandpass to reduce the thermal noise in it.
2. Set the target standard deviation for the observation and estimate the approximate integration time.
3. Acquire test scan data to take the SAV and TAV to decide $N_{\rm sw}$ at the bottom of the SAV.
4. Derive the ON-OFF duty cycle of $(1-x)$:x, based on $N_{\rm sw}$.
5. Estimate the time scale of the stability, and determine the OFF-source-scan interval.
6. Design the optimal ON-OFF scan pattern, based on the time stability of the bandpass and the ON-OFF duty cycle.
7. Apply the bandpass calibration of $H_0(\nu)$ for observed ON- and OFF-source spectra before integration. Employ the spectral smoothing for the OFF-source spectra with a smoothing window of $N_{\rm sw}$.
8. Apply the bandpass calibration of H_1 for ON-source spectra using the adjacent smoothed OFF-source spectra. Time-integrate the bandpass-calibrated ON-source spectra.
9. Apply the baseline subtraction, if necessary, to the OFF-source-subtracted spectrum, and obtain the final result.

[2] Here, we omit overhead and scan gaps for the sake of simplicity.

3. Tests and Results

Field tests have been carried out to investigate whether the SBC works efficiently. We used the VLBI Exploration of Radio Astrometry (VERA: Kobayashi et al. 2003) Iriki 20 m antenna in the single-dish mode. The antenna was pointed at the zenith during the period of our tests. The 22 GHz HEMT receiver was tuned at 22.235 GHz with a bandwidth of 512 MHz. The received signal was downconverted with the first local oscillator (LO) of 16.8 GHz, and the second LO of 5179 MHz before being digitized at 1024 Mbps 2-bit quantization by the digital sampler ADS-1000 (Nakajima et al. 2001). The digital filter unit (Iguchi et al. 2005) was used for splitting the signal into sixteen 16 MHz streams, from which we adopted only the first stream. Spectroscopy was employed by the software spectrometer, VESPA (VEra SPectrum Analyzer: H. Beppu et al. 2011),[3] which produces 1024 ch by 2048-point FFT. This produces a squared sinc spectral resolution function, whose first null appears at the adjacent ch, i.e., $\nu_{\rm sp} = \nu_{\rm res}$.

The template bandpass, $H_0(\nu)$, was obtained on 2010 April 15 for 230 min integration. A 10 hr observation was conducted on 2010 October 5, half-a-year after acquiring the template bandpass to include seasonal variation. A pseudo ON-OFF scan pattern was produced from the 10 hr continuous observation; OFF-source scans were pilfered from the continuous zenith observations. Data quality was checked via monitoring the total power of every spectrum. The first 50 min data were not used because of unexpected operations of hot-load insertion. We also flagged out 3 s data because of obviously irregular spectra, probably due to a data transmission error. Finally, we obtained 32768 s continuous spectra. For the calculation of SAV, we did not use the first spectral channel that includes a direct current (DC) component affected by a voltage bias offset at the digital sampler.

In this test, we set the target standard deviation of the antenna temperature of 50 mK, which is the standard of the regular monitoring program in the VERA Iriki single-dish observation. This corresponds to $\sigma/T_{\rm sys} = 5 \times 10^{-4}$ for $T_{\rm sys} = 100$ K.

We employed 3rd-order B-spline smoothing for OFF-source spectra in step 7, described in subsection 2.3. Node intervals were set to be equal to the smoothing window, $N_{\rm sw}$. The statistical package R was used for data analyses of integration, bandpass calibration, AV calculation, and B-spline smoothing. All of source codes for these procedures are presented in GitHub.[4]

3.1. Bandpass Spectra

The template bandpass, $H_0(\nu)$, is shown in figure 2. The standard deviation of its random noise was 1.97×10^{-5}, which was estimated by $H_0(\nu)/\bar{H}_0(\nu) - 1$, where $\bar{H}_0(\nu)$ was a B-spline-smoothed spectrum. We used $\bar{H}_0(\nu)$ in the following tests, though the standard deviation was smaller than the target noise level by one order of magnitude, in quest of the ultimate performance.

Bandpass-corrected spectra, $T_{\rm OFF}(\nu,t)/\bar{T}_{\rm OFF}\bar{H}_0(\nu) - 1$, are shown in figure 3. Here, $\bar{T}_{\rm OFF}$ is the mean value of the OFF-source spectra that represents $T_{\rm sys}$. Thus, the bandpass-corrected spectrum indicates $H_1(\nu,t)[1 + \epsilon(\nu,t)]/\bar{H}_0(\nu) + \epsilon(\nu,t)$. The solid line in figure 3 was computed by 3rd-order B-spline smoothing with the node intervals, $N_{\rm sw} = 45$, and represents, $\bar{H}_1(\nu,t)/\bar{H}_0(\nu)$. Departures from the solid line were dominated by the thermal noise, $\{1 + [H_1(\nu,t)/H_0(\nu)]\}\epsilon(\nu,t) \simeq \epsilon(\nu,t)$. The smoothed spectrum was time variable. Its time variability is described in subsection 3.3.

3.2. Spectral Allan Variance

The SAVs of bandpass-corrected spectra defined as equation (9) are shown in figure 4. At every frequency channel separation, the SAV decreased with integration time. While the SAV was decreasing as a function of frequency channel separation at shorter integration than 16 s, there appeared a local bottom and a top for longer integration than 16 s. They appeared at < 200 ch and ~ 259 ch, respectively. Figure 5 shows the SAV of a 64 min-integrated spectrum as an example. The profile was composed of two power-law components. For narrower channel separations than the bottom, the SAVs were dominated by a power-law profile with an index of -2.003 ± 0.001. The index above the bottom was 1.29 ± 0.02. The bottom of the SAV appeared near the frequency span where the two power-law components were equivalent.

The bottom shifted toward a narrower spectral separation in a longer integration time, while the top stayed at almost the same separation. These behaviors are summarized in table 1.

3.3. Time Stability

Figure 6 displays the variability of $\bar{H}_1(\nu,t)/\bar{H}_0(\nu)$. The smoothed spectrum shows time variation in terms of not only the power level, but also its shapes, such as the slope, curvature, and local bumps. The variation of the bandpass was evaluated by the standard deviation of the smoothed spectrum, $\sigma_{\rm t}(\nu)$, defined as

$$\sigma_{\rm t}^2(\nu) = \left\langle \left(\frac{\bar{H}_1(\nu,t)}{\bar{H}_0(\nu)} \right)^2 \right\rangle - \left\langle \frac{\bar{H}_1(\nu,t)}{\bar{H}_0(\nu)} \right\rangle^2. \quad (14)$$

Here, the expectation is derived by time average.

Figure 7 shows the standard deviation of the smoothed spectrum. Two clear peaks appeared at 71 ch and 920 ch, near the shoulders of the bandpass, $H_0(\nu)$. The standard deviation of $\sim 2\%$ was significantly greater than the target accuracy of $\sigma/T_{\rm sys} = 5 \times 10^{-4}$. Hence, it is necessary to calibrate the bandpass using the smoothed OFF-source spectrum within the time scale while $\bar{H}_1(\nu,t)/\bar{H}_0(\nu)$ is sufficiently stable.

The time scale of the stability was evaluated by using the TAV defined by equation (13). Since the top and bottom channels of the smoothed bandpass were also time variable, we instead used the twin peak channels in $\sigma_{\rm t}(\nu)$, i.e., we substituted $\Delta H_1(t)$ with $[H_1(71\,{\rm ch},t) - H_1(921\,{\rm ch},t)]$. The TAV is shown in figure 8. The first bottom of the 30 s integrated spectrum appeared at 300 s. The power-law index of the TAV was ~ -2 for $\tau < 60$ s, and -1.7 at $\tau = 80$ s, which we regulate as the spectral stability time scale in following processes.

[3] Beppu, H., Kameno, S., Mizuno, I., Namikawa, D., Takeda, K., Nishida, Y., & Hirota, T. 2011, in VLBI Consortium Symposium (Koganei: NICT) (in Japanese) ⟨http://www2.nict.go.jp/aeri/sts/stmg/vcon/symposium2011/Beppu_Vcon2011VESPA.pdf⟩.

[4] ⟨https://github.com/kamenoseiji/BPsmooth⟩.

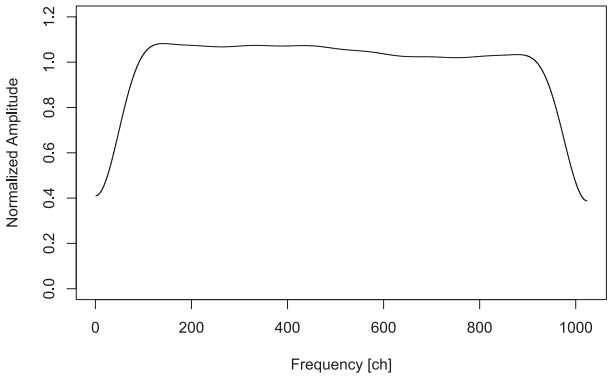

Fig. 2. Template bandpass spectrum, $H_0(\nu)$, obtained by 230 min integration on 2010 April 15. The DC bias (spectrum at ch = 1) is flagged out. The amplitude is normalized as the mean becomes unity.

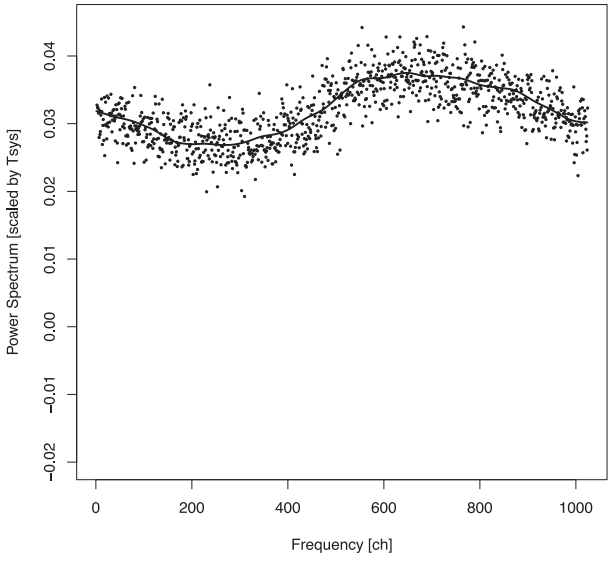

Fig. 3. Bandpass-corrected spectrum, $T_{\rm OFF}(\nu,t)/\bar{T}_{\rm OFF}\bar{H}_0(\nu) - 1 = H_1(\nu,t)/\bar{H}_0(\nu)$ for 10 s average. The solid line shows the smoothed spectrum, $\bar{H}_1(\nu,t)/\bar{H}_0(\nu)$, with the smoothing window of 45 ch.

3.4. Scan Patterns and Performance

Based on the above results, we set the new scan pattern and compared it with the conventional ON-OFF scans without spectral smoothing. The conventional pattern (case 1) consists of pairs of 30 s ON and 30 s OFF scans. The new scan pattern (case 2) was a set of 70 s ON and 10 s OFF with the SBC. The pattern was designed as the cycle period to be shorter than the spectral stability time scale of 80 s and the optimal ON-to-OFF integration time ratio described in equation (10) with $N_{\rm sw} = 45$.

To reach the targeted noise level of $\sigma/T_{\rm sys} = 5 \times 10^{-4}$, the conventional pattern required 20 sets (1200 s) of the total telescope time. Its resultant spectrum is shown in figure 9 (A1). The case-2 spectrum with a telescope time of 1200 s (15 sets of 80 s scans) is shown in figure 9 (C1). The standard deviation was $(2.8^{+0.3}_{-0.2}) \times 10^{-4}$ (median, minimum, and maximum of 27 samples), $\times\, 1/1.74$ that of the conventional scan pattern.

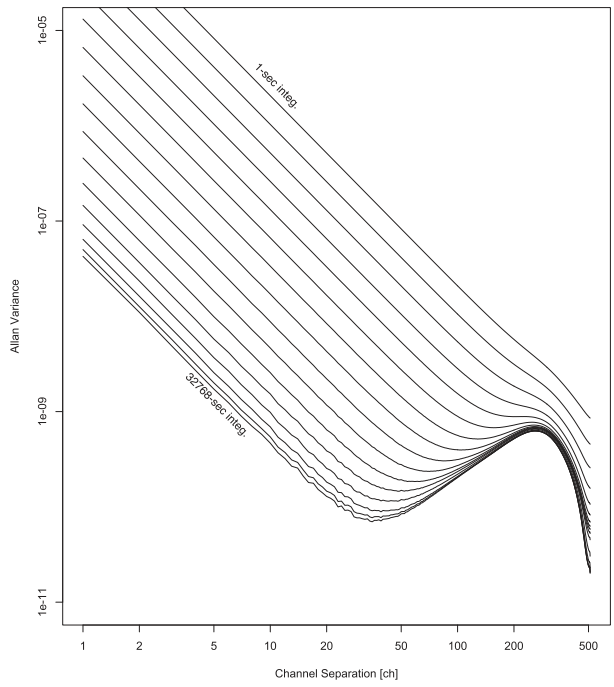

Fig. 4. SAVs across the bandwidth under time integration of 1, 2, 4, …, 32768 s.

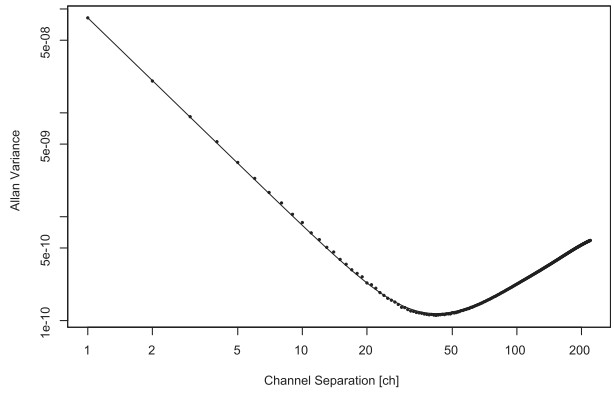

Fig. 5. SAV at 64 min integration. The solid line indicates the best fit with two power-law components; $\sigma_y^2(\nu) = a_1\nu^{\alpha_1} + a_2\nu^{\alpha_2}$. The best-fit power indices are $\alpha_1 = -2.003 \pm 0.001$ and $\alpha_2 = 1.29 \pm 0.02$.

To reach the targeted noise level, case 2 required 5 sets (400 s). Its resultant spectrum is shown in figure 9 (B1).

Since the resultant spectrum presented some wiggled features other than the random noise, we attempted baseline fitting and its subtraction using the 3rd-order B-spline function with a node interval of 45 ch. After baseline subtraction, the standard deviations of case 1, 2 (1200 s), and 2 (400 s) became $(4.7^{+0.3}_{-0.2}) \times 10^{-4}$, $(2.6^{+0.2}_{-0.2}) \times 10^{-4}$, and $(4.5^{+0.3}_{-0.3}) \times 10^{-4}$, respectively, and shown in figure 9 (A2, C2, and B2).

The performance of standard deviations as a function of the total telescope time is summarized in table 2 and figure 10. At any total telescope time, the SBC gave higher performance than conventional scans. While the standard deviation of conventional scans had such dependence on the integration

Table 1. Bottom and top appeared in the SAV.

Integ. (min)	Bottom (ch)	Bottom SAV $\times 10^{-10}$	Top (ch)	Top SAV $\times 10^{-10}$
1	128	5.3	255	7.2
2	103	4.0	257	7.0
4	86	3.1	259	6.8
8	71	2.4	259	6.7
16	60	1.9	259	6.7
32	49	1.4	259	6.5
64	42	1.1	259	6.5
128	39	0.9	259	6.4
256	34	0.7	259	6.3
512	32	0.6	259	6.3

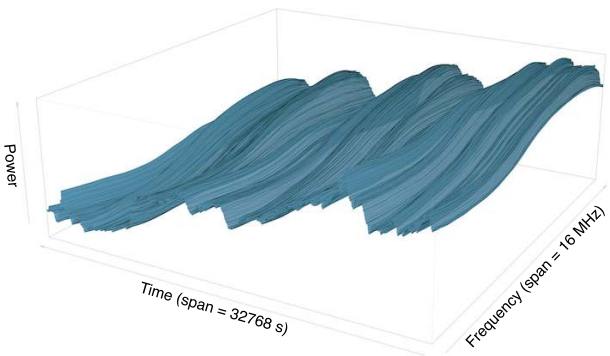

Fig. 6. Time variation of the bandpass-corrected spectrum, $\bar{H}_1(\nu,t)/H_0(\nu)$. Each spectrum was time-averaged for 30 s and spectral-smoothed with a 45 ch B-spline window.

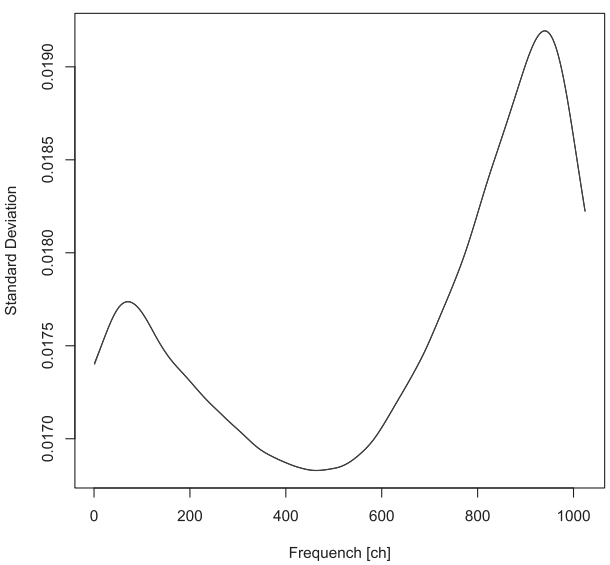

Fig. 7. Standard deviation of each spectral channel in the bandpass-corrected spectrum, $\sigma_t(\nu) = \sqrt{\{\langle[\bar{H}_1(\nu,t)/H_0(\nu)]^2\rangle - \langle\bar{H}_1(\nu,t)/H_0(\nu)\rangle^2\}}$. The spectrum was time-averaged for 30 s and spectral-smoothed with a 45 ch B-spline window before calculation of the standard deviation. Two peaks in the standard deviation appeared at the frequency channels of 71 and 920.

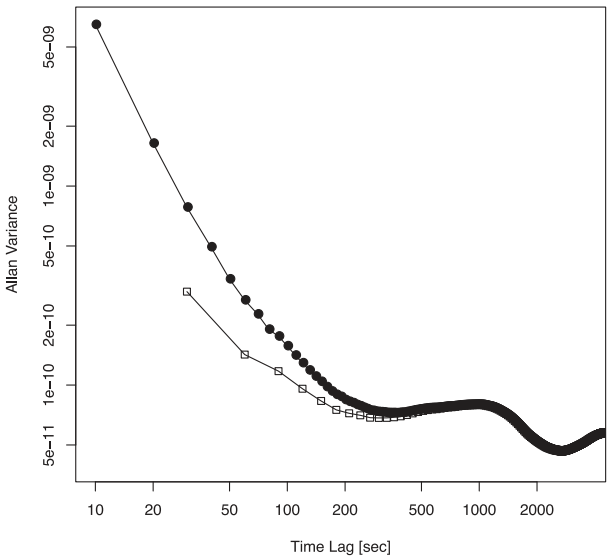

Fig. 8. Time-based Allan variance (TAV), $\sigma_y^2(\tau)$, of the spectral difference between 71 ch and 920 ch as a function of the time lag, as defined by equation (13). Sequences of filled circles and open squares represent 10 s and 30 s time-integrated spectra, respectively. Their local TAV minima appeared at 370 s and 300 s, respectively. A significant departure from the power-law index of -2 arose at $\tau \gtrsim 60$ s.

Table 2. Spectral performance as a function of total telescope time.*

$t_{\rm tot}$	$\sigma/T_{\rm sys}$ ($\times 10^{-4}$)			
(min)	Case 1a	Case 1b	Case 2a	Case 2b
4	$10.8^{+3.7}_{-0.8}$	$10.8^{+0.6}_{-0.7}$	$6.1^{+0.5}_{-0.4}$	$5.7^{+0.5}_{-0.4}$
8	$7.7^{+2.2}_{-0.5}$	$7.5^{+0.4}_{-0.4}$	$4.3^{+0.4}_{-0.3}$	$4.1^{+0.3}_{-0.2}$
16	$5.4^{+1.1}_{-0.4}$	$5.3^{+0.3}_{-0.3}$	$3.1^{+0.3}_{-0.2}$	$2.9^{+0.2}_{-0.1}$
32	$3.88^{+0.28}_{-0.25}$	$3.75^{+0.16}_{-0.20}$	$2.25^{+0.11}_{-0.08}$	$2.07^{+0.11}_{-0.10}$
64	$2.76^{+0.03}_{-0.14}$	$2.66^{+0.04}_{-0.10}$	$1.63^{+0.05}_{-0.11}$	$1.49^{+0.06}_{-0.05}$
128	$1.93^{+0.05}_{-0.03}$	$1.88^{+0.006}_{-0.016}$	$1.19^{+0.05}_{-0.04}$	$1.07^{+0.02}_{-0.01}$
256	$1.33^{+0.01}_{-0.01}$	$1.29^{+0.002}_{-0.003}$	$0.89^{+0.01}_{-0.01}$	$0.78^{+0.02}_{-0.02}$
512	0.93	0.91	0.70	0.59

* Cases with "a" and "b" stand for before and after baseline subtraction, respectively.

time $\sigma \propto t_{\rm integ}^{-0.5}$, the SBC resulted in a shallower slope with a power index of -0.46.

3.5. *Smoothing Window*

The optimal spectral smoothing window, $\Delta\nu$, was determined by the bottom in the SAV listed in table 1. For a time scale longer than 16 min, a bottom appeared at $\Delta\nu/\nu_{\rm sp} \sim 32$–60 ch. We chose the window of 45 ch for time stability tests and spectral performance tests in previous subsections. We also tested the spectral performance with various windows of 2, 3, 4, …, 191 ch on the scan pattern of case 2 with total telescope times of 400 and 1200 s.

Figure 11 shows the results. The median value of standard deviations in the resultant spectrum before baseline subtraction

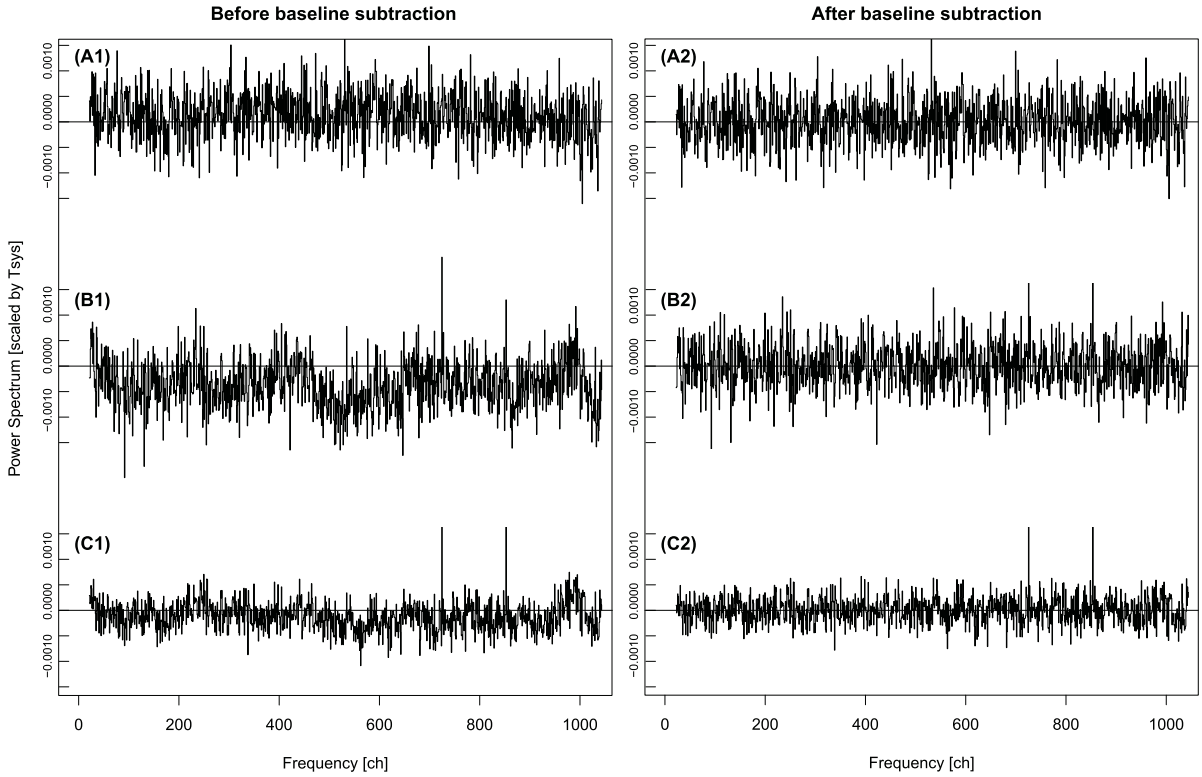

Fig. 9. Resultant spectra after a bandpass correction. Left and right panels stand for before and after baseline subtraction performed after a bandpass correction was applied. A1 and A2: conventional ON-OFF scans (case 1) of the total telescope time of 1200 s. B1 and B2: 70 s ON + 10 s OFF scans with spline smoothing (case 2) with the total telescope time of 400 s. C1 and C2: case-2 scans with the telescope time of 1200 s.

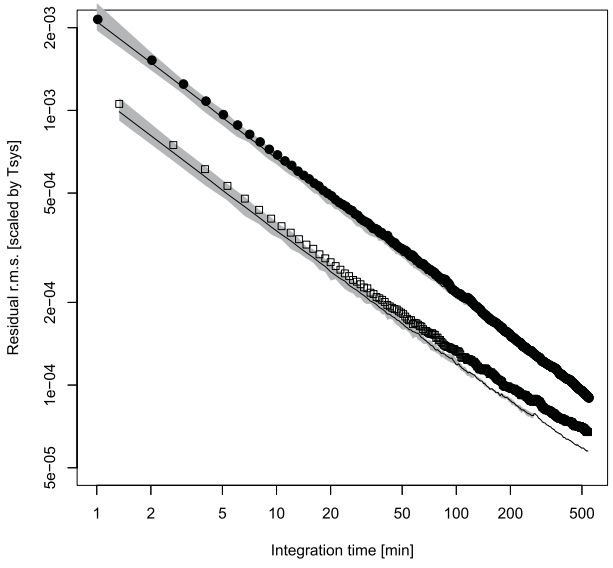

Fig. 10. Standard deviations of the resultant spectra derived by ON-OFF scans as a function of the total telescope time. Filled circles indicate the results from sets of conventional 30 s ON + 30 s OFF scans without spectral smoothing. The opened squares represent those of 70 s ON + 10 s spline-smoothed OFF scans. The solid lines indicate median values of standard deviations obtained after baseline subtraction. The median was taken from a number of sets in 10 hr observations. The gray shade indicates the maximum and minimum values of the sets. While the power-law index of the median values (solid lines) in conventional scans was −0.50 through integration times ranging between 60 and 32400 s, that in the proposed scan was −0.46 between 80 and 32400 s.

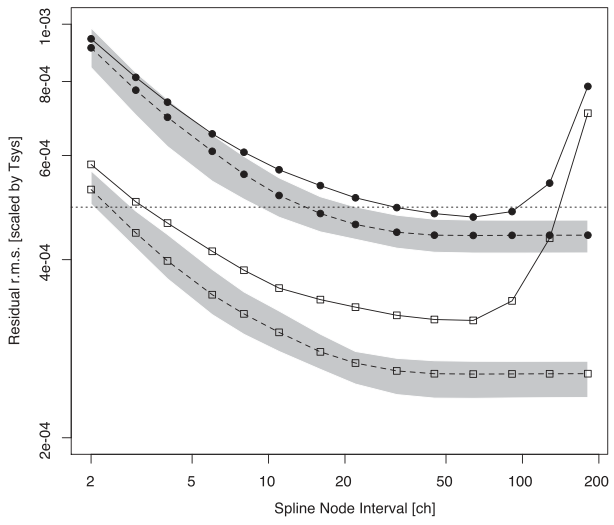

Fig. 11. Standard deviations of the OFF-source-subtracted spectra. Filled circles and opened squares stand for scan patterns of case 2 with telescope times of 400 s and 1200 s, respectively. Solid and dashed lines indicate standard deviations before and after baseline correction with 45 ch spline smoothing, respectively. The horizontal dotted line shows the standard deviation level of case 1 (conventional ON-OFF scans without spectral smoothing). Median values are plotted by symbols. The gray shades indicate the bottom-to-peak range of the baseline-subtracted standard deviations.

recorded a minimum at the 64 ch window for the two telescope times of 400 s and 1200 s. After baseline subtraction, the standard deviation became significantly lower and the minimum appeared as a flat bed for wider windows than 45 ch. In all cases the bottom was smaller than the targeted noise level.

4. Discussion

4.1. Bandpass Flatness

As shown in figure 1, the SAV across the bandwidth is composed of thermal noise and fluctuation of the bandpass characteristics. The crossover point, where the thermal noise and the bandpass fluctuation are equivalent, appears at the bottom of the SAV. The relevant smoothing window, $\Delta\nu$, should be set around the crossover point. For a longer integration time, the bottom of SAV shifts toward a narrower channel separation. The regression of the crossover point indicates that the channel separation of the bottom is related to the integration time as $\Delta\nu_{\rm bottom} \propto t_{\rm integ}^{-0.273\pm0.005}$ for $t_{\rm integ} < 128$ min.

This behavior is explained by the following consideration. The thermal-noise component is stochastic, which does not depend on time and frequency. Thus, the SAV of thermal-noise component is $\propto \Delta\nu^{-2} t_{\rm integ}^{-1}$. The bandpass fluctuation SAV is $\propto \Delta\nu^{1.29\pm0.02}$. This power-law index is slightly steeper than SAV $\propto \Delta\nu$, which is expected for a random-walk process along frequency. Since the bandpass characteristics are frozen during the short time scale, the SAV of the bandpass fluctuation is independent of $t_{\rm integ}$. Therefore, the crossover point appears under the condition of $\Delta\nu^{-2} t_{\rm integ}^{-1} = \alpha \Delta\nu^{1.29}$ where α is a proportional coefficient. Thus, the SAV bottom will appear at $\Delta\nu_{\rm bottom} \propto t_{\rm integ}^{-\frac{1}{3.29}}$. The behavior of the test observation, which indicates $\Delta\nu_{\rm bottom} \propto t_{\rm integ}^{-0.273\pm0.005}$, is consistent with the theoretical consideration.

Although a different combination of a receiving system and a spectrometer other than the VERA system may have different properties of bandpass flatness, measuring SAVs at various integration times allows us to decompose them into thermal-noise and random-walk components.

4.2. Expected Time Reduction

As shown in subsection 3.4, the SBC (case 2) allows us to shorten the total telescope time to $1/3$ to attain the targeted noise level, as compared with the conventional method (case 1). In other words, the SBC reduces the standard deviation by a factor of $\sqrt{3}$ within the same total telescope time. These results demonstrate that the telescope-time efficiency can be tripled by the SBC method with the optimal scan pattern.

Since our analysis did not take the scan-gap time into consideration, the efficiency can be different from that in realistic observations. As shown in figure 9, systematic undulation remains in the case-2 spectrum before baseline subtraction. The undulation can be ascribed to a time interval of 70 s between OFF-source scans, which may be longer than the stability time scale (see figure 8). Although OFF-scan intervals should be shorter to reduce the undulation, this modification increases the time loss in scan gaps. The optimal scan pattern should be tested in detail under realistic conditions of the scan gaps and the time stability.

As shown in figure 10, the slope of standard-deviation reduction by time integration for the SBC was shallower than that for conventional scans. The shallower slope indicates that the SBC underperforms at a long integration time. This underperformance can be caused by the time instability of the bandpass. The power index of the TAV of -1.7 at $\tau = 80$ s, with a small departure from -2, indicates that the bandpass fluctuation remains at a level of $\sigma_{\rm y} \sim 10^{-5}$ (see figure 8). This level of fluctuation is not tangible in conventional scans, even at the longest integration ($\sigma/T_{\rm sys} = 9.3 \times 10^{-5}$), but can be substantial in the SBC ($\sigma/T_{\rm sys} = 6.3 \times 10^{-5}$). The bandpass stability can be the principal component to determine the sensitivity at a longer integration time than 32400 s. To pursue the sensitivity at longer integrations, a shorter scan pattern should be considered in spite of time loss in the scan gaps.

4.3. Advantages in a Dual Beam System

Dual-beam systems are equipped in some radio telescopes, such as the GBT 100 m (Jewell 2002), the Nobeyama 45 m (Kuno et al. 2010), and the VERA (Kobayashi et al. 2003), to double the time efficiency by interchanging two beams between ON- and OFF-source scans. The duty cycle for ON and OFF scans in dual-beam systems should be 1:1, or $x = 0.5$ in equation (11), if the performances of two receivers are uniform, though it is different from the optimal duty cycle for the SBC. In this case, the variance, σ^2, will be reduced by a factor of $[1 + (1/N_{\rm sw})]/2$ when we employ the SBC. Taking $N_{\rm sw} = 45$ for instance, the variance is reduced by a factor of 0.51, and the telescope-time efficiency is almost doubled, 3.9 times better than conventional ON-OFF scans with a single beam system, or 1.3 times better than the SBC with a single beam system.

Consideration in this subsection implies that the SBC for a single beam with conventional ON-OFF scans (1:1 duty cycles) also doubles signal-to-noise ratio. A reanalysis with the SBC for previous observations can offer an opportunity to enhance signal-to-noise ratio, if ON- and OFF-source spectra are separately recorded, and the efficiency depends on the spectral stability of the system.

4.4. Advantages in OTF Scans

ON-the-fly (OTF) mapping shares the OFF-source pointing among a continuous scan pass (Mangum et al. 2007). Sawada et al. (2008) argued that the noise level achieved in the unit observing time of the OTF map is written as

$$\Delta T_{\rm A}^{*}(0) = \frac{T_{\rm sys}}{\sqrt{B}} \sqrt{\left(\frac{1}{t_{\rm cell}^{\rm ON}} + \frac{1}{t_{\rm cell}^{\rm OFF}}\right)} \times \sqrt{\left(t_{\rm scan} + t_{\rm OH} + \frac{t_{\rm OFF}}{N_{\rm scan}^{\rm SEQ}}\right) N_{\rm row} f_{\rm cal}}, \quad (15)$$

where B is the frequency resolution of the spectrum and $f_{\rm cal}$ is the overhead of R-SKY calibration, and they derived the optimal OFF-source integration time, $t_{\rm OFF}$, to map a rectangular area with a row span of l_1;

$$t_{\rm OFF} = \sqrt{(t_{\rm scan} + t_{\rm OH}) \frac{\eta d t_{\rm scan}}{l_1}} \sqrt{N_{\rm scan}^{\rm SEQ}}, \quad (16)$$

where $t_{\rm scan} = l_1/v_{\rm scan}$ is the ON-source scan time for a row by the scan speed of $v_{\rm scan}$, $t_{\rm OH}$ the overhead time between row scans, η the efficiency determined by the gridding convolution function, d the grid spacing, and $N_{\rm scan}^{\rm SEQ}$ the number of row scans between OFF-source integrations. In the practical case of $\eta = 4.3$, $l_1 = 600''$, $\Delta l = 5''$, $d = 7\farcs5$, $t_{\rm OH} = 25$ s, and $N_{\rm scan}^{\rm SEQ} = 1$ according to Sawada et al. (2008), the ON-source scan times of $t_{\rm scan} = 20$, 40, and 60 s yield $t_{\rm OFF}^{\rm optimal} = 7$, 12, and 17 s, respectively.

The optimization is modified when the SBC is applied. Equation (15) is modified into

$$\Delta T_{\rm A}^*(0) = \frac{T_{\rm sys}}{\sqrt{B}} \sqrt{\left(\frac{1}{t_{\rm cell}^{\rm ON}} + \frac{1}{N_{\rm sw} t_{\rm cell}^{\rm OFF}}\right)} \times \sqrt{\left(t_{\rm scan} + t_{\rm OH} + \frac{t_{\rm OFF}}{N_{\rm scan}^{\rm SEQ}}\right) N_{\rm row} f_{\rm cal}}, \quad (17)$$

when the smoothing window is $N_{\rm sw}$ ch. The optimal OFF-source integration will be

$$t_{\rm OFF} = \sqrt{(t_{\rm scan} + t_{\rm OH}) \frac{\eta d t_{\rm scan}}{N_{\rm sw} l_1}} \sqrt{N_{\rm scan}^{\rm SEQ}}. \quad (18)$$

When compared with Sawada et al. (2008), $t_{\rm scan} = 20$, 40, and 60 s yield $t_{\rm OFF}^{\rm optimal} = 1$, 1.8, and 2.5 s when we take $N_{\rm sw} = 45$, and their noise levels decrease by factors of 0.886, 0.874, and 0.856, respectively. Thus, the total telescope time that achieves the same standard deviation will be reduced by a factor of $\sim$1.3–1.4.

The effect of the SBC is less than simple ON-OFF scans; nevertheless, the SBC offers somewhat better results. Consideration in this subsection does not involve the bandpass fluctuation. More realistic optimization and noise level should be estimated based on the time stability of the receiving system.

4.5. Vulnerability to Spurious Signals

The SBC method shows weakness in undesirable spurious emissions, such as radio frequency interference, contamination of sampling clocks and reference signals in a receiving system, artificial pattern caused by numerical errors of spectral calculation, etc. These spurious signals usually show spiky features in both ON- and OFF-scan spectra. They are suppressed in the smoothed OFF-scan spectra, while kept in the unsmoothed ON-scan spectra. Thus, they will appear in the final results, though they would be subtracted by the conventional ON-OFF scans if they are stable.

In our test observations, spurious emissions appeared at 704 ch and 832 ch (see figure 9) that correspond to 11/16 and 13/16 of the bandwidth, respectively. Their line widths are narrower than the spectral resolution. Digital noise, such as harmonics of the sampling clock, can cause such spurious emissions whose frequencies are simple fractions of the bandwidth. These spurious frequencies should be masked in the process of data reduction. Observers need to pay close attention to spurious emissions when they apply the SBC method.

5. Summary

It is presented that the proposed SBC method offers significantly better performance than conventional ON-OFF scans, especially when a stable spectrometer, such as a digital system, is equipped. Our tests showed that the total telescope time was reduced to 1/3 to attain the same signal-to-noise ratio, or $\times$ 1.7 better signal-to-noise ratio was obtained in the same telescope time for single-pointing ON-OFF scans. The SBC method was also efficient for dual-beam systems and ON-the-fly mapping.

The optimal analysis scheme of the SBC is presented in this paper. To apply this method, radio observatories should offer:

- Long-time integrated bandpass to obtain a sufficiently good $H_0(\nu)$. This can be done in off seasons.
- SAV to show flatness of $H_1(\nu, t)$ in order to allow observers to compute the optimal smoothing window.
- TAV to estimate the stability time scale of $H_1(\nu, t)$ in order to design the optimal scan pattern and total telescope time required.
- Spectral outputs of ON- and OFF-sources, separately. Automated ON-OFF subtraction makes it impossible to OFF-source spectral smoothing in postobservation analysis.

Finally, reanalysis of previous spectral data with the SBC can also offer an opportunity to enhance signal-to-noise ratio, if ON- and OFF-source spectra are separately recorded.

The VERA Iriki 20 m telescope is a part of the VERA VLBI network that is operated by the National Astronomical Observatory of Japan and staffs and students of the Kagoshima University.

References

Iguchi, S., Kurayama, T., Kawaguchi, N., & Kawakami, K. 2005, PASJ, 57, 259
Jewell, P. R. 2002, in Proc. URSI General Assem. (Maastricht, the Netherlands: URSI), 1959
Kobayashi, H., et al. 2003, ASP Conf. Ser., 306, 367
Kuno, N., et al. 2010, Abstract, Astron. Soc. Japan Autumn Meeting, V45a (in Japanese)
Mangum, J. G., Emerson, D. T., & Greisen, E. W. 2007, A&A, 474, 679
Nakajima, J., Koyama, Y., Sekido, M., Kurihara, N., Kondo, T., Kimura, M., & Kawaguchi, N. 2001, Exp. Astron., 11, 57
Sawada, T., et al. 2008, PASJ, 60, 445
Wilson, T. L., Rohlfs, K., & Hüttemeister, S. 2009, Tools of Radio Astronomy (Berlin: Springer), 69